


Short-wavelength excitation two-photon intravital microscopy of endogenous fluorophores

TING WU,^{1,2,3} JIULING LIAO,^{1,3} FENG XIANG,^{1,3}  JIA YU,^{1,3}
YUFENG GAO,^{1,3} LINA LIU,^{1,3} SHIWEI YE,^{1,3} HUI LI,^{1,3,6} KEBIN
SHI,^{4,5,7} AND WEI ZHENG^{1,3,8}

¹Research Center for Biomedical Optics and Molecular Imaging, Shenzhen Institute of Advanced Technology, Chinese Academy of Sciences, Shenzhen 518055, China

²University of Chinese Academy of Sciences, No.19(A) Yuquan Road, Shijingshan District, Beijing 100049, China

³Shenzhen Key Laboratory for Molecular Imaging, Guangdong Provincial Key Laboratory of Biomedical Optical Imaging Technology, Shenzhen Institute of Advanced Technology, Shenzhen 518055, China

⁴State Key Laboratory for Mesoscopic Physics and Frontiers Science Center for Nano-optoelectronics, School of Physics, Peking University, Beijing 100871, China

⁵National Biomedical Imaging Center, Peking University, Beijing 100871, China

⁶hui.li@siat.ac.cn

⁷kebinshi@pku.edu.cn

⁸zhengwei@siat.ac.cn

Abstract: The noninvasive two-photon excitation autofluorescence imaging of cellular and subcellular structure and dynamics in live tissue could provide critical *in vivo* information for biomedical studies. However, the two-photon microscopy of short-wavelength endogenous fluorophores, such as tryptophan and hemoglobin, is extremely limited due to the lack of suitable imaging techniques. In this study, we developed a short-wavelength excitation time- and spectrum-resolved two-photon microscopy system. A 520-nm femtosecond fiber laser was used as the excitation source, and a time-correlated single-photon counting module connected with a spectrograph was used to provide time- and spectrum-resolved detection capability. The system was specially designed for measuring ultraviolet and violet-blue fluorescence signals and thus was very suitable for imaging short-wavelength endogenous fluorophores. Using the system, we systematically compared the fluorescence spectra and fluorescence lifetimes of short-wavelength endogenous fluorophores, including the fluorescent molecules tyrosine, tryptophan, serotonin (5-HT), niacin (vitamin B3), pyridoxine (vitamin B6), and NADH and the protein group (keratin, elastin, and hemoglobin). Then, high-resolution three-dimensional (3D) label-free imaging of different biological tissues, including rat esophageal tissue, rat oral cheek tissue, and mouse ear skin, was performed *in vivo* or *ex vivo*. Finally, we conducted time-lapse imaging of leukocyte migration in the lipopolysaccharide injection immunization model and a mechanical trauma immunization model. The results indicate that the system can specifically characterize short-wavelength endogenous fluorophores and provide noninvasive label-free 3D visualization of fine structures and dynamics in biological systems. The microscopy system developed here can empower more flexible imaging of endogenous fluorophores and provide a novel method for the 3D monitoring of biological events in their native environment.

© 2023 Optica Publishing Group under the terms of the [Optica Open Access Publishing Agreement](#)

1. Introduction

Endogenous fluorophores, which are fluorescent biomolecules inherent in tissues, can provide fluorescent probing without perturbing the biological environment. Three-dimensional (3D) imaging of endogenous fluorophores could allow for the noninvasive *in vivo* inspection of vital

biological processes, such as metabolic changes, morphological alterations, and disease progress [1]. Therefore, the visualization of endogenous fluorophores has attracted much attention in the past decades, and many striking results have been obtained in biomedical research [2,3]. However, the 3D imaging of short-wavelength endogenous fluorophores that are in the ultraviolet (UV) or violet-blue wavelength bands, such as tryptophan, keratin, and hemoglobin, still presents challenges despite significant progress in fluorescence imaging techniques.

Single-photon excitation autofluorescence imaging methods, such as epi-fluorescence microscopy [4], confocal microscopy [5], and structured illumination microscopy [6], require UV wavelength light to excite the short-wavelength endogenous fluorophores. The UV light usually causes short penetration depth and a poor signal-to-noise ratio due to the considerable light scattering in turbid tissue. Furthermore, the UV radiation-induced damage to biological samples cannot be ignored, especially for *in vivo* studies. Therefore, single-photon excitation is not a good choice for the fluorescence imaging of short-wavelength endogenous fluorophores.

Two-photon excitation fluorescence microscopy (TPEM), which inherently requires excitation light with a wavelength nearly twice that of the one-photon excitation for a given fluorophore, has evolved as a powerful intravital imaging tool for biomedical research [7,8]. TPEM has several advantages, such as the 3D fluorescence imaging of living cells deep within thick, strongly scattering samples and reduced phototoxicity and photodamage [9, 10]. However, the most commonly used TPEM excitation source, Ti: sapphire femtosecond lasers, can only provide light beyond 700 nm [11], which exhibits low excitation efficiency for UV fluorophores [12]. Therefore, most previous uses of TPEM for endogenous fluorophores focused on the reduced nicotinamide adenine dinucleotide (NADH, absorption maxima at 730 nm) and the flavin adenine dinucleotide (FAD, absorption maxima at 850 nm), which emit visible fluorescence [13].

To excite UV fluorophores, several strategies have been developed to obtain short-wavelength femtosecond light, including the optical parametric oscillator (OPO) [14] or supercontinuum generation from a photonic crystal fiber (PCF) [15]. Unfortunately, these methods all require a pump source such as a Ti: sapphire laser, and the OPO system itself is sophisticated, bulky, and expensive. Moreover, supercontinuum generation using a PCF is susceptible to environmental variables, such as temperature and pump power, which easily result in unstable output power. This will significantly affect the imaging fidelity because the two-photon excitation fluorescence signal quadratically depends on the excitation power. To date, the need for a compact, stable, and low-cost femtosecond light source for TPEM imaging of short-wavelength endogenous fluorophores remains unmet.

In addition to efficient excitation, specific detection is also critical for fluorescence imaging. However, the fluorescence spectra that are commonly used as indicators to identify different fluorophores are usually broad and overlap with each other for short-wavelength endogenous fluorophores. The fluorescence lifetime, which is defined as the average time a molecule spends in an excited state before returning to its relaxed ground state, provides complementary information for characterizing different fluorophores in the time domain. Therefore, the combination of spectrum-resolved detection and time-resolved detection could empower the exact interrogation of endogenous fluorophores [16], although it has not yet been systematically explored in the short-wavelength band.

In this study, a short-wavelength excitation time- and spectrum-resolved TPEM system was constructed. A compact and stable mode-locked fiber laser with a center wavelength of 520 nm was equipped as the excitation source to efficiently excite the short-wavelength endogenous fluorophores, and a time-correlated single-photon counting (TCSPC) module connected to a spectrograph was used to detect the fluorescence spectra and fluorescence lifetime simultaneously. Using this system, we systematically assessed the fluorescence lifetime and spectral characteristics of pure chemical samples, including the fluorescent molecules tyrosine, tryptophan, serotonin (5-HT), niacin (vitamin B3 (VB3)), pyridoxine (vitamin B6 (VB6)), and NADH, and the

protein groups of keratin, elastin, and hemoglobin, which comprise the typical short-wavelength endogenous fluorophores in biological tissues. Next, we explored the distribution of the short-wavelength endogenous fluorophores in the esophageal wall based on their unique spectral and lifetime characteristics. Finally, we performed 3D imaging of mouse skin and rat oral mucosa and captured leukocyte migration in the mouse ear pinna *in vivo* based on short-wavelength endogenous fluorophores. The dynamics of leukocyte recruitment and accumulation in the microenvironment of typical immune responses (lipopolysaccharide [LPS] injection or mechanical trauma) were elucidated. We believe that this study could substantially extend the flexibility of 3D autofluorescence imaging and provide a novel means for the noninvasive TPEM of biological samples and events.

2. Materials and methods

2.1. Microscope setup

In this study, a short-wavelength excitation time- and spectrum-resolved TPEM system was constructed. A home-built short-wavelength mode-locked femtosecond laser was used as the excitation source. The details about the laser can be found in our previous work [17]. In brief, based on a 1040-nm self-phase modulated mode-locked fiber laser, 520-nm short-wavelength femtosecond laser pulses were generated by laser frequency doubling with a lithium triborate (LBO) nonlinear crystal. The pulse repetition frequency was 60.7 MHz, the pulse duration was 106 fs, and the maximum average output power was about 500 mW.

The system diagram is shown in Fig. 1(a). First, the 520-nm laser beam exiting the home-built laser was raster scanned by two galvanometer mirrors (TSH-8203 M, Sunny Technology, China), which were conjugated by a relay system (L1 and L2), for two-dimensional imaging. After the scanning, the laser beam passed through a scan lens (CLS-SL, Thorlabs), a tube lens (AC254-200-B, Thorlabs), and a dichroic mirror (FF510-Di01, Semrock), and then was focused on the sample by a water immersion objective (UApoN340, 40 \times , NA 1.15, Olympus). The epifluorescence signals were collected by the same objective and split from the excitation laser with the dichroic mirror above. Furthermore, the residual excitation light was removed with a band-pass filter (FF01-405/150-25, Semrock). After the filter, the fluorescence signals were conducted to a spectrograph via a fiber bundle for spectral recording. The detector of the spectrograph was a 16-channel linear-array photomultiplier tube (PMT, PML-16-0-C, Becker & Hickl GmbH). The 16 channels covered a spectral range of 300–500 nm with an interval of 12.5 nm. Finally, a time-correlated single-photon counting module (TCSPC, SPC-150NX, Becker & Hickl GmbH) was connected to the detector to record the fluorescence decay curve of each spectral band into 256-time channels. The full width at half maximum (FWHM) of the system's instrument response function was ~ 220 ps, which was measured by recording the reflected femtosecond laser pulses. For 3D imaging, the imaging depth was controlled by axially translating the objective using an actuator.

To improve the fluorescence collection efficiency of the microscopy system, the back aperture of the objective lens was conjugated to the end face of the aforementioned fiber bundle using a specially designed 4f system (L3 and L4 in Fig. 1(a)). The 4f system consisted of a pair of fused silica single lenses with focal lengths of 200 mm (L3) and 35 mm (L4). In addition, to avoid the interference of 520 nm laser-excited fluorescence noise from sample immobilization equipment, this work used low-autofluorescence, transparent, and colorless coverslips (CG15KH, Thorlabs) in sample preparation.

The imaging resolution was measured using 0.1- μm diameter microspheres (F8797, Thermo Fisher Scientific). Figure 1(b) and (c) show the five microspheres' average intensity profiles in the x-y and x-z planes. The profiles were fitted with the Gaussian function and the extracted FWHMs were 245 nm and 423 nm for the x-y and x-z planes, respectively. The imaging field of view was 256 $\mu\text{m} \times 256 \mu\text{m}$. The z-scanning step size of 3D imaging was 3 μm . The fluorescence

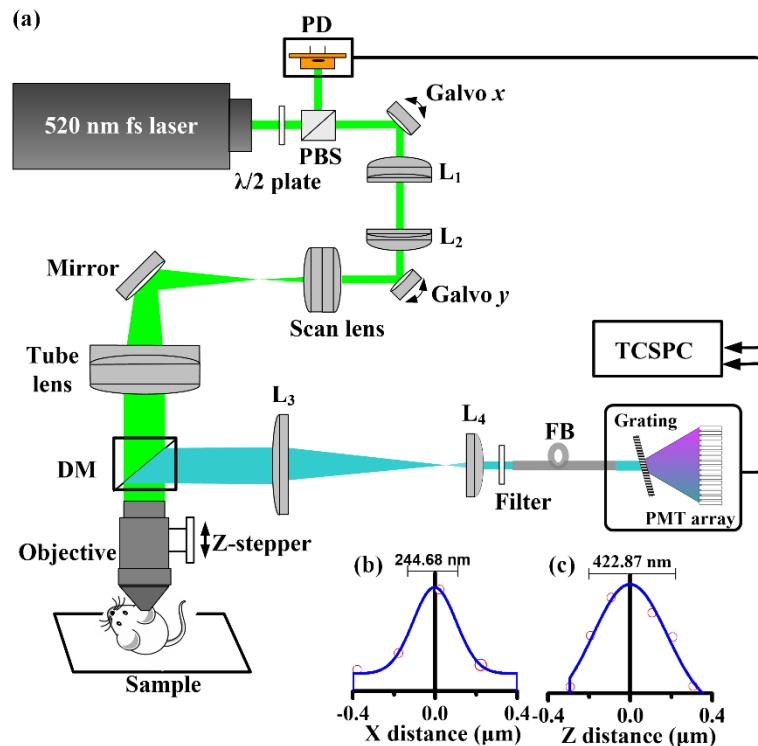


Fig. 1. (a) Scheme of the short-wavelength excitation time- and spectrum-resolved two-photon microscope. PBS, polarization beam splitter; L, lens; DM, dichroic mirror; FB, fiber bundle; PMT, photomultiplier tube; TCSPC, time-correlated single-photon counting. (b) The lateral and (c) axial resolutions were measured using 0.1 μm -diameter microspheres.

collection time of each frame of time- and spectrum-resolved image with 256×256 pixels was 8 s for *in vitro* imaging and 16 s for *in vivo* imaging to guarantee a high signal-to-noise ratio. The excitation power is about 2–5 mW for the pure fluorophore measurement and about 10–60 mW for the biological tissue measurement. To overcome the attenuation of the excitation light by the tissue, the laser power was gradually increased with increasing imaging depth. The maximal laser power after the objective was controlled at <60 mW at the largest imaging depth of $\sim 183 \mu\text{m}$ (Fig. 4(f)). There was no obvious photodamage or photobleaching observed during the experiment.

2.2. Preparation of the pure samples of endogenous fluorophores

To obtain the accurate fluorescence spectra and lifetime characteristics of short-wavelength endogenous fluorophores, the pure chemical samples of the main intrinsic biological emitters in the UV or violet-blue wavelength bands were measured. These compounds were tryptophan, tyrosine, serotonin (5-HT), niacin (VB3), pyridoxine (VB6), NADH, keratin, elastin, and hemoglobin. For measurement, 4 mg tryptophan (T0254, Sigma-Aldrich), 1 mg tyrosine (T3754, Sigma-Aldrich), 1 mg serotonin (bs-1126P, Bioss), 50 mg pyridoxine (BN20262, Biorigin), 20 mg NADH (10107735001, Sigma-Aldrich), 10 mg niacin (N814566, Macklin), and 50 mg elastin (E920946, Macklin) were dissolved in 1 mL phosphate-buffered saline (PBS, pH 7.2) individually. A 5% keratin solution (K862557, Macklin) was directly purchased and measured.

Hemoglobin was extracted from the blood of BALB/c mice as previously reported [15]. First, the red blood cells were washed with a large amount of PBS and centrifuged at a low speed of

3000 rpm to make the large red blood cells sink to the bottom. Next, plasma and other impurities were removed from the upper layer of the centrifuge. Third, deionized water and toluene were added to the red blood cell solution in a volume ratio of 1:1:0.4 to release the hemoglobin in red blood cells. After standing for 24 hours, the solution was centrifuged at a high speed of 15,000 rpm, and the underlying hemoglobin solution was collected for measurement.

2.3. Preparation of the tissue samples

For *ex vivo* experiments, fresh esophageal tissues and oral tissues were excised from adult WKY rats (12-week-old, male) after euthanasia. The sample surface was washed with PBS several times to remove the impurities such as food residue. Then, the sample was sandwiched between a coverslip and a microscope slide for imaging while immersed in PBS to prevent dehydration.

For *in vivo* experiments, BALB/c mice (6-week-old, male) were used and normal and stimulated mouse ear skin were imaged. Specifically, the mice were anesthetized using the intraperitoneal injection of ketamine (100 mg/kg) and xylazine (15 mg/kg) mixture. Then, depilatory cream was utilized on the ear skin to remove the hair and thus exclude the interference signal from the hairs. Afterward, the ear was washed with PBS and flattened on the sample table using double-sided tape. Finally, the skin was gently covered with a coverslip for imaging.

Stimulation was induced after ear immobilization and before covering the coverslip. Two kinds of stimulations were performed in this study to establish immunization models. The first stimulation was the LPS injection. As described in the previous study [18], 10 μ g LPS was subcutaneously injected into the mouse ear pinna to induce inflammation. The second stimulation was mechanical trauma, in which the ear pinna was pricked using a needle stick gently without obvious bleeding.

For each imaging study, at least three independent experiments were performed, and all the experimental procedures were approved by the Institutional Animal Care and Use Committee, Shenzhen Institute of Advanced Technology (Ethics Approval No. SIAT-IACUC-20210304-YGS-SWGXYJZX-LH-01).

2.4. Data analysis

For the spectral analysis of the chemical samples, the spectral curves were obtained by integrating the photons in each channel of the PMT arrays. For the spectral analysis of biological tissues, spectrum-coded images were created according to the following strategy. First, a specific RGB color was assigned to a given spectral channel. Second, the color-weighted intensity image of the channel was calculated by multiplying the intensity of each pixel with the RGB color. Third, the 16 color-weighted intensity images were combined to obtain a spectrum-coded image. The abovementioned analyses were performed using custom MATLAB programs.

For fluorescence lifetime analysis, the measured fluorescence decay curve ($F(t) = f(t) * R(t)$) was deconvolved with the instrument response function of the imaging system ($R(t)$) and subsequently fitted with a single-exponential decay function ($f(t) = a_1 e^{-\frac{t}{\tau_1}}$) for small-molecule chemical samples or a bi-exponential decay function ($f(t) = a_1 e^{-\frac{t}{\tau_1}} + a_2 e^{-\frac{t}{\tau_2}}$) for protein chemical samples and biological samples. In these equations, τ_1 and τ_2 are the time-decay constants, while a_1 and a_2 are the respective amplitudes of the decay terms. The mean fluorescence lifetime is defined as $\tau_m = (\alpha_1 \tau_1 + \alpha_2 \tau_2) / (\alpha_1 + \alpha_2)$. The fluorescence lifetime-coded images were produced with SPCImage software (Becker & Hickl).

3. Results

3.1. Spectral and temporal characteristics of short-wavelength endogenous fluorophores

In this study, a 520-nm excitation time- and spectrum-resolved TPEM system for imaging of short-wavelength endogenous fluorophores was constructed. To assess the availability of the system and obtain the accurate fluorescence characteristics of short-wavelength endogenous fluorophores upon 520-nm two-photon excitation, this work systematically measured and compared the fluorescence spectra and fluorescence lifetimes of the main intrinsic biological emitters in the UV or violet-blue wavelength bands. These fluorophores included tryptophan, tyrosine, serotonin (5-HT), niacin (VB3), pyridoxine (VB6), NADH, keratin, elastin, and hemoglobin. Tyrosine and tryptophan are aromatic amino acids that exist in many types of proteins [8,12]. Serotonin is the indoleamine derivative of tryptophan [19]. Serotonin is a chemical messenger that is believed to act as a mood stabilizer. NADH is a kind of coenzyme that acts as an electron donor in oxidation-reduction reactions. Niacin (VB3) is a precursor of NADH. Pyridoxine is a form of VB6 that is necessary to properly function sugars, fats, and proteins in the body. Elastin and keratin are fibrous proteins that provide structural support for cells and tissues. Hemoglobin is a protein in red blood cells that carries oxygen. Our previous study found that 520-nm femtosecond light effectively excited the two-photon fluorescence of hemoglobin [17].

The aforementioned fluorophores were divided into two groups: the small molecule group, which consisted of tyrosine, serotonin (5-HT), tryptophan, niacin (VB3), pyridoxine (VB6), and NADH, and the protein group, which consisted of keratin, elastin, and hemoglobin. The normalized fluorescence spectra of the small molecules and the proteins are shown in Fig. 2(a) and (b), respectively. The fluorescence spectra of small molecules were relatively simple and stable. For example, the emission peak of tryptophan was at 350 nm, and the emission peak of tyrosine was below 320 nm, which was consistent with the literature [20]. As a tryptophan derivative, serotonin showed a tryptophan-like fluorescence emission with a peak at about 335 nm. The maximum fluorescence emission peaks of VB3 and VB6 were 420 nm and 400 nm, respectively, which was consistent with previous reports that vitamins and their derivatives had visible fluorescence (400–500 nm) [8]. NADH also exhibited a blue fluorescence emission maximum at 450 nm, which was probably due to the reduced nicotinamide ring of NADH [21].

Compared with the stable fluorescence spectra of small molecules, the fluorescence spectra of proteins were more complicated due to the complex molecular energy structure. Usually, the fluorescence emission peak of proteins varies with the excitation wavelength [1,22]. For example, previous studies reported that the fluorescence of keratin peaked at 350 nm upon one-photon excitation at 275 nm and peaked at 440 nm upon excitation at 350 nm [23]. In this study, the fluorescence emission peak of keratin was located at 340 nm under two-photon excitation of 520 nm, which was blue-shifted compared with the one-photon excitation of 275 nm. The cause of this result was not fully understood, but this finding was probably due to the complex aromatic amino acid fluorescent cross-linking in the protein structure as reported in the literature [24]. Similar to keratin, elastin also has cross-links in its structure [25]. The measurement obtained in the present study showed that elastin exhibited an emission maximum at 400 nm and a small peak at 480 nm under two-photon excitation of 520 nm. The 400-nm peak resembled that of VB6. This was mainly due to the fact that both elastin and VB6 have the pyridinoline group, which exhibits a 400-nm emission maximum upon one-photon excitation at the UV band [26]. The small peak at 480 nm may have corresponded to pyridinoline aggregates [8,27]. The fluorescence emission spectrum of hemoglobin exhibited two peaks under 520 nm excitation. One was located at 435 nm, which was consistent with our previous study [15], and the second was located at about 340 nm. The second peak was probably associated with the presence of aromatic amino acids in hemoglobin [28,29].

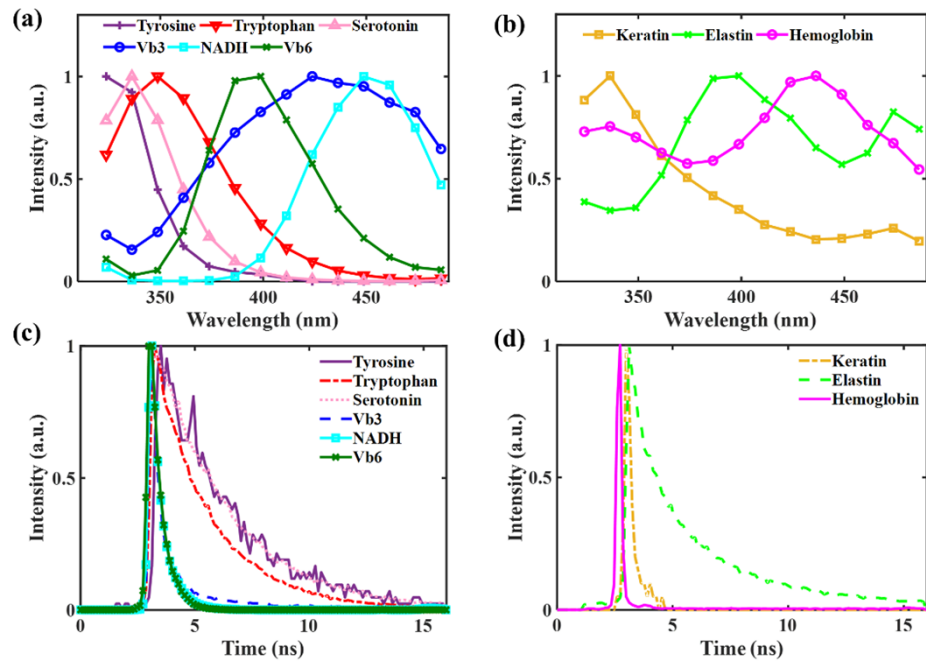


Fig. 2. Fluorescence characteristics of short-wavelength endogenous fluorophores. (a) Fluorescence spectra of small molecules. (b) Fluorescence spectra of proteins. (c) Fluorescence intensity decay curves of small molecules. (d) Fluorescence intensity decay curves of proteins. Vb3, vitamin B3 or niacin; Vb6, vitamin B6 or pyridoxine.

In addition, the fluorescence lifetime can provide complementary information about the molecular configuration and the microenvironment. Figure 2(c) and (d) show the fluorescence intensity decay curves of the fluorophores mentioned above. To calculate the fluorescence lifetime, the fluorescence decays of small molecules could be fitted using a single-exponential model, whereas the decays of proteins should be fitted with a bi-exponential model considering their complex structure. Table 1 summarizes the calculated fluorescence lifetime values. It was obvious that tyrosine, tryptophan, and serotonin had relatively long fluorescence lifetimes at 3.0 ns, 2.4 ns, and 3.2 ns, respectively, whereas VB3 and VB6 and their derivatives like NADH exhibited a short lifetime of ~ 0.5 ns. These results were consistent with previous reports [19,30–34]. However, keratin exhibited a short lifetime of 0.24 ns in the experiment, which was different from the previously reported 1.4 ns [35]. This was probably due to the difference in pH values. The keratin solution used in the present study was directly purchased from Macklin, and its pH was ~ 5.6 . Elastin had a long fluorescence life of 2.17 ns with a short lifetime component of 0.78 ns (close to the fluorescence lifetime of vitamins) and a long lifetime component of 3.54 ns (close to the fluorescence lifetime of amino acids). This indicated that in addition to vitamin (pyridinoline) cross-links, there were other luminescent cross-links, which may have been amino acid cross-links, in the elastin [8,25]. Hemoglobin showed an extremely short fluorescence lifetime that was close to the detector response time, consistent with the previous study [15].

These results suggest that the 520 nm excitation time- and spectrum-resolved TPTEM system developed herein can enable the specific characterization of short-wavelength endogenous fluorophores, and the measured fluorescence characteristics of pure fluorophores would provide an important reference and guidance for the label-free imaging of biological tissues and events.

Table 1. Fluorescence lifetime values of short-wavelength endogenous fluorophores.

Chemical	Concentration	τ_m (ns)
Tyrosine	PBS: 1 mg/mL	3.04
Tryptophan	PBS: 4 mg/mL	2.44
Serotonin	PBS: 1 mg/mL	3.16
VB3	PBS: 10 mg/mL	0.62
NADH	PBS: 20 mg/mL	0.52
VB6	PBS: 50 mg/mL	0.49
Keratin	5%	0.24 ($\tau_1 = 0.10$, $\tau_2 = 1.76$)
Elastin	PBS: 50 mg/mL	2.17 ($\tau_1 = 0.78$, $\tau_2 = 3.54$)

3.2. Identifying short-wavelength endogenous fluorophores in the epithelial tissue

After testing on pure fluorophores, we further attempted to identify the short-wavelength endogenous fluorophores in biological tissues. The esophageal wall, which has a complex layered structure with abundant structural components, including epithelial cells, muscle fibers, collagen fibers, and elastin fibers (Fig. 3(a)), is an ideal tissue for exploring and interpreting endogenous fluorophores in epithelial tissues. The inner surface of the esophageal wall is the keratinized epithelium (KE) formed due to the long-term mechanical friction with food. Underlying the KE is a layer of nonkeratinized flat epithelium called the stratified squamous epithelium (SE). Further down is the lamina propria (LP), with loose connective tissue and abundant capillaries. Adjacent to LP is the muscularis propria (MP), which creates the wave-like peristalsis that moves food boluses down the esophagus and into the stomach. Underlying the MP is the fibrosa (FB), the outermost layer of the esophageal wall (Fig. 3(a)). Figure 3(b) shows corresponding autofluorescence TPEM images of each layer of the esophageal wall. The TPEM intensity images (the left column in Fig. 3(b)) only provided general morphological features, whereas the spectral and lifetime images (the middle and right columns in Fig. 3(b)) provided detailed structures, such as the elastin fibers (green, ROI3 and ROI6) and blood vessels (red, ROI4) in the LP layer.

In addition to morphological information, the spectral and lifetime images also revealed the biochemical properties of the esophagus. The KE, SE, and MP layers were found to have very similar fluorescence spectra with the maximum emission peaks concentrated at 335 nm (Fig. 3(c)). This emission peak was mainly attributed to tryptophan, which is widely present in tissues as an important protein building block. However, there was a blue shift between these spectra compared with the spectrum of the pure chemical tryptophan (Fig. 3(d)). The cause of this difference was not fully understood, although it may have been due to the effect of the tissue microenvironment, which can change the fluorescence quantum yield, spectral peak position, and line width [22]. It should be emphasized that, rather than the keratin aqueous solution, the keratin-filled epithelial cells, including keratinocytes (ROI1) and squamous cells (ROI2), showed characteristic spectra more consistent with that of tryptophan despite the blue shift (Fig. 3(d)). This may have been attributed to the tryptophan residues present in the protein [36], suggesting that keratinization did not change the tryptophan residues in esophageal epithelial cells. By contrast, there was another weak emission peak around 400 nm in the LP and FB layers, except for the 335 nm emission peak of tryptophan (Fig. 3(c)). The weak peak may have been contributed by the elastin because it was similar to the emission spectrum of pure elastin, although with a blue shift (Fig. 3(e)). Notably, NADH is also present in cells, but very little NADH fluorescence was observed in the esophageal tissue (Fig. 3(c)), indicating that NADH exhibited a much weaker emission compared with tryptophan under 520-nm excitation.

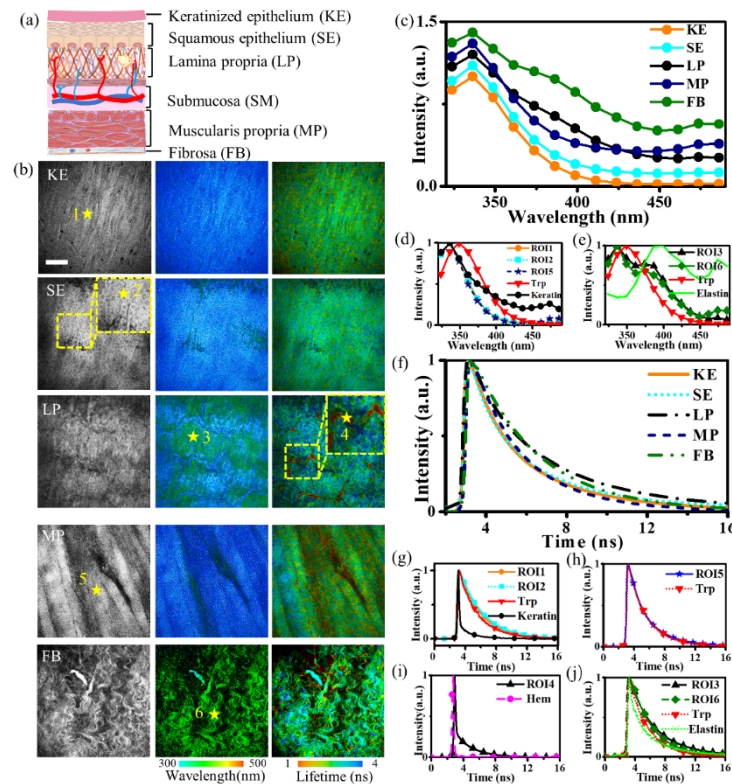


Fig. 3. Identifying short-wavelength endogenous fluorophores in the esophageal wall. (a) The layered structure of the esophageal wall. (b) Autofluorescence two-photon microscopy images of each layer of the esophageal wall (left column: intensity images; middle column: color-coded spectral images; right column: color-coded lifetime images). The KE, SE, and LP layers were measured from the inner surface outwards, while the MP and FB were measured from the outer surface inwards. Scale bar: 50 μm . Six different regions of interest were selected from different layers: keratinocytes (ROI1), squamous epithelial cells (ROI2), blood vessels (ROI4), elastin fibers (ROI3 and ROI6) and muscle fibers (ROI5). (c) The fluorescence spectra of each layer. (d) Comparison of fluorescence spectra between keratinocytes (ROI1), squamous epithelial cells (ROI2), and muscle fibers (ROI5) with pure keratin and tryptophan. The ROIs were marked out by the yellow stars in (b). (e) Comparison of fluorescence spectra between elastin fibers (ROI3 and ROI6 marked out by the yellow stars in (b)) with pure tryptophan and elastin. (f) Fluorescence intensity decay curves of each layer. (g) Comparison of fluorescence intensity decay curves between keratinocytes (ROI1) and squamous epithelial cells (ROI2) with pure keratin and tryptophan samples. (h) Comparison of fluorescence intensity decay curves between muscle fibers (ROI5) and pure tryptophan sample. (i) Comparison of fluorescence intensity decay curves between vessels (ROI4) and pure hemoglobin (Hem) sample. (j) Comparison of fluorescence intensity decay curves between elastin in ROI3 and ROI6 with pure tryptophan and elastin samples.

In addition to the fluorescence spectra, the fluorescence intensity decays (reflecting the fluorescence lifetime information) of different layers of the esophageal wall were analyzed (Fig. 3(f)). Similar to the spectra, the fluorescence lifetimes of the KE, SE, and MP layers were nearly the same, while the fluorescence lifetimes of LP and FB were relatively longer. By comparing the findings with the fluorescence decay curves of pure chemicals, it was inferred that the autofluorescence of KE, SE, and MP mainly came from tryptophan, whereas the sources of

LP and FB autofluorescence were tryptophan and elastin (Fig. 3(g), (h), and (j)), as demonstrated by the fluorescence spectra above (Fig. 3(d) and (e)). The slight difference in fluorescence lifetimes between keratinocytes (ROI1, KE), squamous cells (ROI2, SE), and muscle fibers (ROI5, MP) with pure tryptophan was ascribed to the different number of tryptophan residues and the interaction between tryptophan residues with neighboring amino acids in different proteins [37]. In addition, abundant vascular structures (ROI4) were distinguished based on their short fluorescence lifetime, which was close to that of hemoglobin, in the LP (Fig. 3(i)), indicating that the hemoglobin was the dominant fluorophore in the blood vessels when excited at 520 nm.

It should be noted that, although the fluorescence spectrum and lifetime usually provide overlapping biochemical information for tissues, they are still highly complementary. For example, compared with the fluorescence spectrum, the fluorescence lifetime of some fluorophores showed stronger consistency between the environment in tissue and pure solution (Fig. 3(d) vs. Figure 3(g) and (h)). The fluorescence lifetime could expose vascular structures in tissues clearly, which was not possible for the fluorescence spectrum (Fig. 3(b) and (i)). Finally, the fluorescence spectrum was superior to the fluorescence lifetime in the determination of the chemical components of mixed fluorophores with distinct spectral peaks because matching characteristic spectral peaks with the corresponding fluorophores was simple and direct (Fig. 3(e) vs. Figure 3(j)). Therefore, integrating the fluorescence spectrum and lifetime could more accurately reveal the biochemical properties of cells and tissues relative to using a single method.

In summary, the abovementioned experimental results illustrate that the combination of the spectrum- and time-resolved signals in the 520 nm-TPEM system developed in this work could better reveal the fine structures (keratinocytes, squamous epithelial cells, elastic fibers, and muscle fibers) and molecular compositions (tryptophan, keratin, elastin, and hemoglobin) of the esophageal wall as well as how they relate to each other.

3.3. High-resolution 3D imaging of skin and mucosa with short-wavelength endogenous fluorophores

To further assess the versatility of the short-wavelength TPEM system for the label-free high-resolution 3D imaging of biological tissues, we captured time- and spectrum-resolved images from mouse skin *in vivo* and rat oral mucosa *ex vivo* without applying any exogenous fluorescence agents. For the mouse skin, the fluorescence intensity images (the top row in Fig. 4) revealed the cellular and subcellular structures at different depths. The spinosum layer composed of flat polygonal cells with large round dark nuclei was observed at a depth of 12 μm from the skin surface (Fig. 4(a)). Below the spinosum layer, the granulosum layer, which has a honeycomb pattern and is located 21–54 μm below the surface, was exposed (Fig. 4(b)). As the imaging depth increased, the next layer, the papillary dermis, appeared from a depth of 57 μm (Fig. 4(c) and (d)). The perforated structure was identified as a hair follicle (white arrows in Fig. 4(b) and (c)). In the dermis, dermal cells (mainly round/elliptical mast cells, yellow arrows in Fig. 4(c) and (d)), and tubular structures (orange arrows in Fig. 4(d)) were seen.

Compared with the intensity images, the color-coded fluorescence spectral and lifetime images (the middle and bottom rows in Fig. 4) provided more detailed information about the biophysical properties of the skin tissue. The fluorescence spectrum peaking at 350 nm indicated that the intracellular fluorescence signal was dominated by tryptophan, which may have originated from protein components in the cytoplasm. From the fluorescence lifetime images, the short lifetime (red color) of hemoglobin made capillaries (magenta arrows in Fig. 4(c)–(e)) distinguishable from the surrounding long-lifetime (green color) tissues compared with the spectrum-resolved images and the intensity images. Even at the greatest imaging depth with significantly blurred tissue morphology, the blood vessels were still easily identified (Fig. 4(f)). The green (long lifetime) tubular structures (orange arrows in Fig. 4(d)) next to the red capillaries may have been lymphatic vessels, which needs to be confirmed with further investigation.

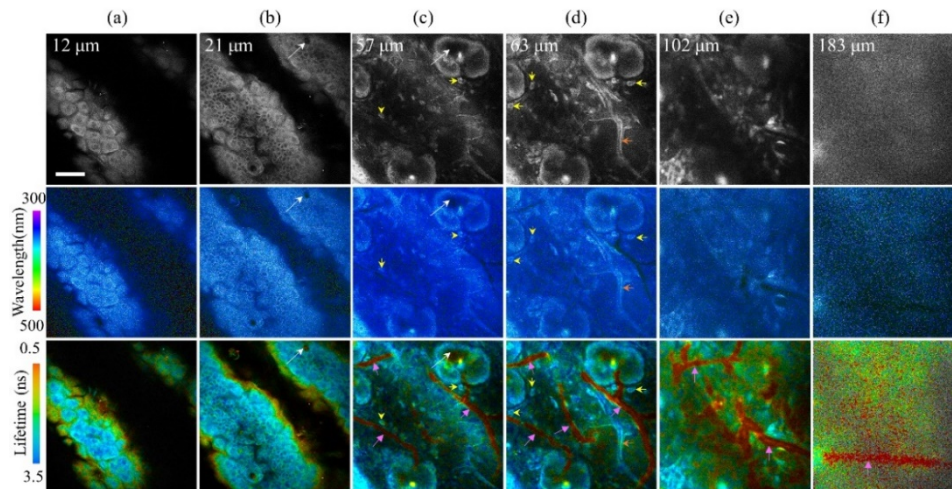


Fig. 4. Three-dimensional autofluorescence two-photon microscopy imaging of mouse skin *in vivo*. Intensity images (top), color-coded spectral images (middle), and color-coded lifetime images (bottom) reveal the structure of the (a) spinosum, (b) basal cell layer, and (c)-(f) dermis (see [Visualization 1](#)). The white, yellow, magenta, and orange arrows point to hair follicles, dermal cells, blood vessels, and suspected lymphatic vessels, respectively. Scale bar: 50 μm .

For the imaging of the rat oral mucosa, the oral cheek tissue was freshly excised from a rat and the tissue facing the cheek pouch was measured. As shown in Fig. 5(a), the outermost layer of the oral mucosa was composed of keratinized cells. At 27 μm below the stratum corneum, the superficial layer of the stratified squamous epithelium was composed of incomplete keratinized flat cells (Fig. 5(b)). Beneath these cells were polygonal spinous layer cells, and the deepest columnar basal layer close to the epidermal-dermal junction appeared at 48 μm below the mucosa surface. At a depth of 72 μm , capillaries were observed in the fluorescence lifetime image (the middle column in Fig. 5(c)).

3.4. Intravital label-free time-lapse imaging of cell motility

3.4.1. Capturing single red blood cells and leukocytes flowing in the microvessels by fluorescence lifetime imaging

Time-lapse imaging of leukocyte dynamics is of great importance for biological studies, especially immunology research. Therefore, an immunization model of LPS injection was created to verify whether the system developed in this work could visualize and identify the leukocytes non-invasively. As shown in Fig. 6, about three hours after the subcutaneous injection of LPS, leukocytes arrested in a blood vessel were captured. The dynamic process of leukocyte arrest took ~ 15 min and was presented by snapshots at six-time points (see details in [Visualization 2](#)). The images have been color-coded with fluorescence lifetime values so that the short fluorescence lifetime appears red, and the long fluorescence lifetime appears blue. As shown in Fig. 6(a) and (b), a short-fluorescence-lifetime (red pseudo-color) red blood cell (R, marked out with magenta circles) and a long-fluorescence-lifetime (blue pseudo-color) leukocyte (L1, marked out with yellow circles) flowed normally in the capillary at the beginning. Once the leukocyte L1 was stagnant in the capillary (Fig. 6(c)), the following red blood cells gradually formed a thrombus behind it (Fig. 6(d)). Subsequently, leukocyte L2 was also blocked (Fig. 6(e) and (f)). These results demonstrate that the efficient two-photon excitation of hemoglobin and tryptophan at 520 nm and the distinct lifetimes of the two fluorophores could significantly facilitate the accurate

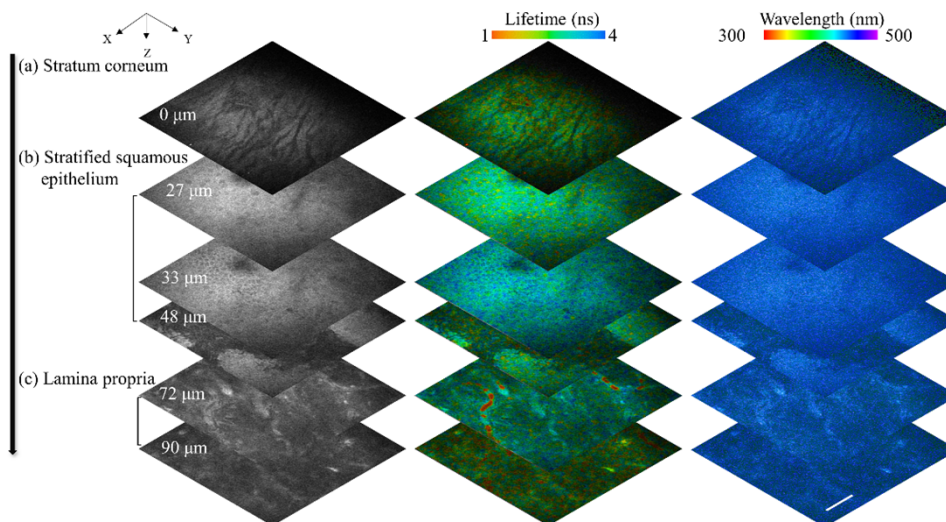


Fig. 5. Two-photon autofluorescence imaging of rat oral mucosa *ex vivo*. (a) Stratum corneum, (b) stratified squamous epithelium, and (c) the lamina propria were shown. Left column: fluorescence intensity images; the middle column: fluorescence lifetime images; the right column: fluorescence spectral images. Scale bar: 50 μm .

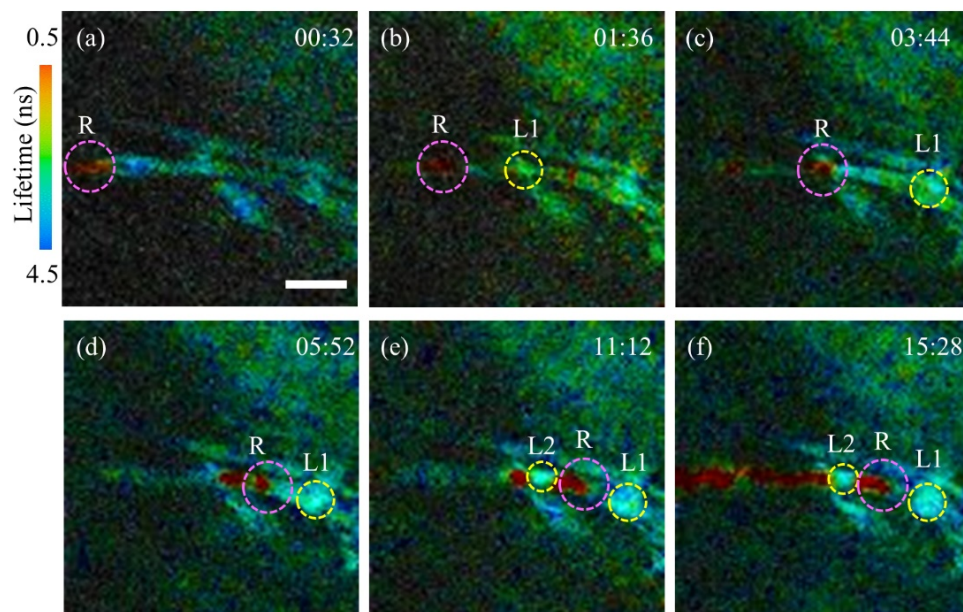


Fig. 6. Time-lapse autofluorescence lifetime imaging of the inflammation microenvironment after LPS subcutaneous stimulation (see [Visualization 2](#)). The arrest of intravascular leukocytes was recorded non-invasively *in vivo*. L1, L2: leukocytes marked with yellow circles; R: red blood cells marked with magenta circles. The time is shown at the corner of each panel as min:s. Scale bar: 20 μm .

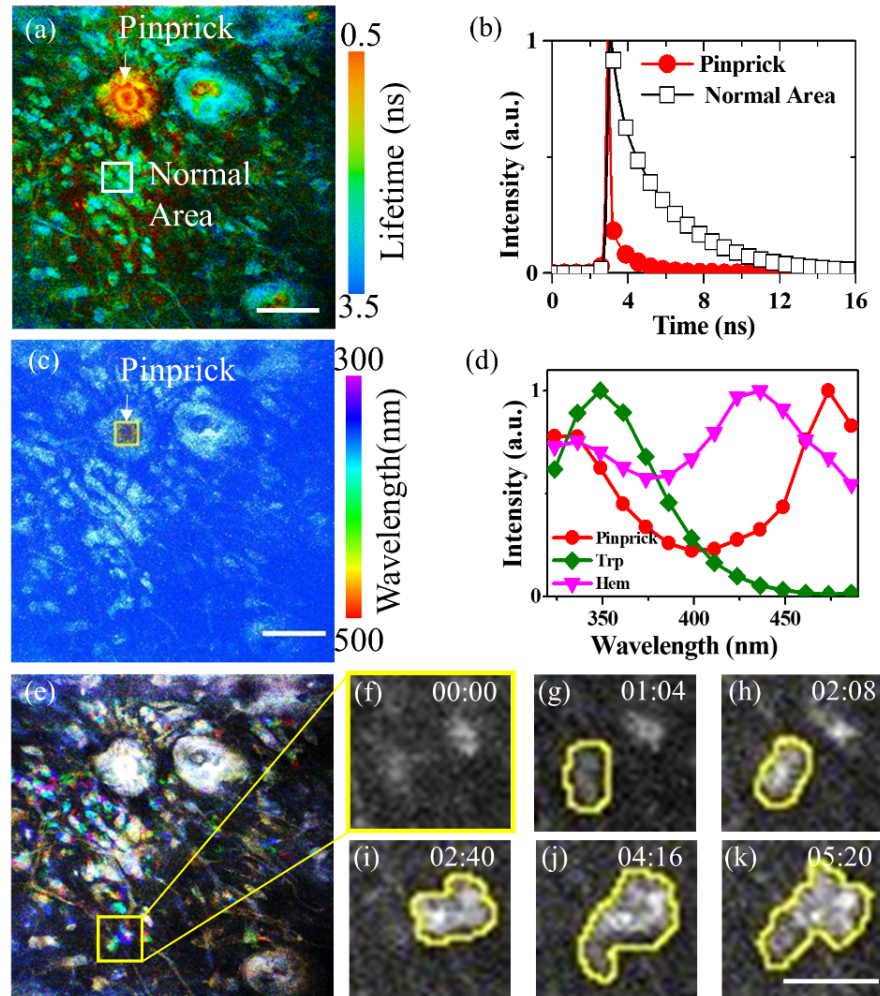


Fig. 7. *In vivo* autofluorescence imaging of the inflammation response post-pinprick challenge in mouse ear pinna. (a) A frame of fluorescence lifetime image of the inflammation microenvironment. Scale bar: 50 μm . (b) Comparison of the fluorescence intensity decay curves of the injured area (indicated by a white arrow) and the surrounding area (marked by a white square). (c) A frame of fluorescence spectral image of the inflammation microenvironment. Scale bar: 50 μm . (d) Comparison of the fluorescence spectral curves of the injured area (indicated by a yellow solid rectangle area), hemoglobin (Hem), and tryptophan (Trp). (e) The multi-color overlay of images recorded at $t_1 = 0$ (red), $t_2 = 02:08$ (green), and $t_3 = 04:16$ (blue) taken from Visualization 3 reveals the active movement of the suspected leukocytes. For static structures, the three colors are superimposed as white, while mobile structures are colorful. (f)–(k) Time-lapse images of the solid rectangle area in (e). Typical amoeboid-manner crawling (f–i) and interaction (j–k) of leukocytes (see Visualization 3 for the full process). The time is shown at the corner of each panel as min:s. Scale bar: 20 μm .

and noninvasive identification and visualization of red and white blood cells *in vivo*. Here, only the fluorescence lifetime images were presented, because the fluorescence lifetime information is already enough to provide easy and clear discrimination between the red blood cells and white blood cells in the capillaries.

3.4.2. Monitoring mobile cells' amoeboid movement and interaction in the interstitial space after mechanical trauma

Mechanical trauma is another important and widely used immunization model. In this study, time-lapse imaging of this kind of model was also performed, and the dynamics of mobile cells' movement and interaction with each other in the dermis after the pinprick challenge of the mouse ear pinna were captured. As shown in Fig. 7(a), the damaged area (indicated by the white arrow) exhibited a remarkably shorter fluorescence lifetime relative to the surroundings. A comparison of the fluorescence intensity decays is presented in Fig. 7(b). Although the causes of the decrease in the lifetime of the injured point were not fully understood, this result was probably due to the leaked hemoglobin from damaged or dilated capillaries. In addition, vasodilation occurred in the area around the injured point, which led to increased blood volume and vascular permeability and thus caused blood leakage from the vessels. As shown in Fig. 7(c) and (d), the spectral curve in the pinpricked area was close to the hemoglobin solution. Moreover, a large number of mobile cells were observed next to the injured area (see Fig. 7(c) and [Visualization 3](#)), which may have been the leukocytes recruited to the wound. Typical amoeboid-manner crawling of these leukocytes and their folding, deforming, and interaction were captured *in vivo* (see Fig. 7(d)–(i) and [Visualization 3](#)). These results further verified the ability of the system developed in this work to monitor immune response in the native tissue environment.

4. Discussion

In this study, a short-wavelength (520 nm) excitation time- and spectrum-resolved TPTEM system was developed that not only enabled the label-free 3D visualization of cellular and subcellular structures but also provided noninvasive time-lapse imaging of dynamic processes in biological systems. Ascribed to the 520-nm excitation, this system efficiently imaged short-wavelength endogenous fluorophores without UV damage, which usually appears in single-photon excitation systems. Furthermore, this system penetrated deeper into biological tissues compared with confocal systems due to its two-photon excitation scheme. Therefore, this system is extremely suitable for the visualization of biological processes in live tissues.

To explore the utility of the system, we first measured and compared the fluorescence characteristics of pure endogenous fluorophores that emit ultraviolet and violet-blue fluorescence, mainly including tryptophan, tyrosine, serotonin (5-HT), niacin (VB3), pyridoxine (VB6), NADH, keratin, elastin, and hemoglobin. The results demonstrate that combining the fluorescence spectrum and lifetime imaging modes in conjunction with the spectral and lifetime analyses could better characterize and discriminate short-wavelength two-photon excited endogenous fluorophores relative to using a single mode. Fluorophores with similar spectra but different fluorescence decay times, such as tryptophan and keratin, elastin and VB6, as well as fluorophores with different spectra but similar fluorescence decays, such as tryptophan and elastin, can be clearly differentiated (Fig. 2). Subsequently, different biological tissues were visualized, including rat esophagus tissue *ex vivo*, rat oral cheek tissue *ex vivo*, and mouse ear skin *in vivo*. The results show that this system can provide high-resolution 3D morphological information as well as physicochemical information for biological systems without administering any extra fluorescent agents.

Moreover, this TPTEM system can be used to noninvasively monitor leukocyte trafficking *in vivo* together with lifetime measurement over time due to its high excitation and detection efficiency of endogenous fluorophores. It should be noted that although the fluorescence intensity image

could visualize the subcellular structures, the fluorescence lifetime information of tryptophan and hemoglobin can be used to distinguish the red and white blood cells as well as the location of the wound and normal tissues. Lin et al. developed a similar TPEM system to image tryptophan fluorescence based on an OPO light source. They demonstrated the capability of the system to perform the label-free imaging of immune cells, including leukocyte trafficking and the immune response of skin mast cells *in vivo* [38–40]. However, the system design was based on intensity detection alone. As a result, it can only provide gray-intensity images without fluorescence spectral and lifetime information. By contrast, the system developed in the present work can provide both morphological and functional information to study complex immune responses in skin inflammatory microenvironments due to its fluorescence spectral and lifetime detection ability. As mentioned above, the fluorescence spectral and lifetime information can serve as important parameters in studying the effect of chemical factors such as pH, ions, and molecularity in biological systems.

In addition, it should be noted that although the system developed herein can image 3D subcellular structures and dynamic microcirculation *in vivo*, the system still has some limitations. First, the imaging depth is limited due to the short wavelength of excitation compared with conventional TPEM, which uses a NIR laser as the excitation source. As a result, only superficial tissues were investigated in this study. This problem may be partially solved by increasing tissue transparency or adopting adaptive optics in future studies. Second, high-NA and high-transmittance objective lenses in the UV band are scarce. The shortest wavelength signal that could be collected using the objective in the present study was about 320 nm, and thus some deep UV signals, such as the second harmonic generation signals of collagen fibers, were lost. We believe that a specially customized UV objective would significantly benefit the performance of our TPEM system. Alternatively, if we combine this visible light TPEM with near-infrared excitation, the imaging capability of the two-photon excitation autofluorescence FLIM system will be extended to almost all known endogenous fluorophores such as NADH, FAD, etc., besides second harmonic generation imaging of collagen fibers. In addition, 520 nm can also excite the one-photon fluorescence of some fluorophores. The combination of one- and two-photon excitation at 520 nm may provide comprehensive detection of endogenous fluorophores. Third, the results presented in this study are all based on non-independent fluorescence spectral and lifetime analysis. In the future, we hope that the data analysis methods would be updated to provide non-overlapping fluorescence spectrum and fluorescence lifetime information. The advance would enable more precise fluorophore identification and more subtle biological studies.

5. Conclusions

In summary, this work developed a short-wavelength (520 nm) excitation time- and spectrum-resolved TPEM system and demonstrated that this system effectively excited and detected short-wavelength endogenous fluorescence signals in biological tissues. We anticipate that the system developed herein could extend the adoption of endogenous fluorophores into blue and even UV bands and provide a novel method for the 3D imaging of biological events in their native environment.

Funding. National Key Research and Development Program of China (2022YFF0712500); National Natural Science Foundation of China (62105353, 81927803, 82071972, 82102106, 92150301, 92159104); the Scientific Instrument Innovation Team of the Chinese Academy of Sciences (GJJSTD20210003); the Shenzhen Basic Research Program (RCJC20200714114433058, RCYX20210609104445093, ZDSY20130401165820357).

Disclosures. The authors declare that they have no competing interests.

Ethics approval and consent to participate. This project complied with all relevant ethical regulations for animal testing and research. All of the experimental procedures were approved by the Institutional Animal Care and Use Committee, Shenzhen Institute of Advanced Technology (Ethics Approval No. SIAT-IACUC-20210304-YGS-SWGXYJZX-LH-01).

Data availability. The datasets used and/or analyzed during the current study are available from the corresponding author upon reasonable request.

References

1. E. Shirshin, B. Yakimov, M. Darvin, N. Omelyanenko, S. Rodionov, Y. Gurfinkel, J. Lademann, V. Fadeev, and A. J. B. Priezzhev, "Label-free multiphoton microscopy: the origin of fluorophores and capabilities for analyzing biochemical processes," *Biochemistry* **84**(S1), 69–88 (2019).
2. V. J. N. M. Marx, "It's free imaging—label-free, that is," *Nat. Methods* **16**(12), 1209–1212 (2019).
3. G. Borile, D. Sandrin, A. Filippi, K. I. Anderson, and F. Romanato, "Label-free multiphoton microscopy: much more than fancy images," *Int. J. Mol. Sci.* **22**(5), 2657 (2021).
4. D. J. Webb and C. M. Brown, "Epi-fluorescence microscopy," in *Cell imaging techniques* (Springer, 2012), pp. 29–59.
5. J. Jonkman, C. M. Brown, G. D. Wright, K. I. Anderson, and A. North, "Tutorial: guidance for quantitative confocal microscopy," *Nat. Protoc.* **15**, 1585–1611 (2020).
6. M. . Gustafsson, "Surpassing the lateral resolution limit by a factor of two using structured illumination microscopy," *J. Microsc.* **198**(2), 82–87 (2000).
7. W. Denk, J. H. Strickler, and W. Webb, "Two-photon laser scanning fluorescence microscopy," *Science* **248**(4951), 73–76 (1990).
8. W. R. Zipfel, R. M. Williams, R. Christie, A. Y. Nikitin, B. T. Hyman, and W. Webb, "Live tissue intrinsic emission microscopy using multiphoton-excited native fluorescence and second harmonic generation," *Proc. Natl. Acad. Sci. U. S. A.* **100**(12), 7075–7080 (2003).
9. W. R. Zipfel, R. M. Williams, and W. W. Webb, "Nonlinear magic: multiphoton microscopy in the biosciences," *Nature Biotechnology* **21**, 1369–1377 (2003).
10. F. Helmchen and W. Denk, "Deep tissue two-photon microscopy," *Nat. Methods* **2**(12), 932–940 (2005).
11. C. Lefort, "A review of biomedical multiphoton microscopy and its laser sources," *J. Phys. D: Appl. Phys.* **50**(42), 423001 (2017).
12. A. A. Rehms and P. R. Callis, "Two-photon fluorescence excitation spectra of aromatic amino acids," *Chem. Phys. Lett.* **208**(3-4), 276–282 (1993).
13. S. Huang, A. A. Heikal, and W. Webb, "Two-photon fluorescence spectroscopy and microscopy of NAD (P) H and flavoprotein," *Biophys. J.* **82**(5), 2811–2825 (2002).
14. M. Ghotbi, A. Esteban-Martin, and M. Ebrahim-Zadeh, "BiB3O6 femtosecond optical parametric oscillator," *Opt. Lett.* **31**(21), 3128–3130 (2006).
15. W. Zheng, D. Li, Y. Zeng, Y. Luo, and J. Qu, "Two-photon excited hemoglobin fluorescence," *Biomed. Opt. Express* **2**(1), 71–79 (2011).
16. D. Li, W. Zheng, and J. . Qu, "Time-resolved spectroscopic imaging reveals the fundamentals of cellular NADH fluorescence," *Opt. Lett.* **33**(20), 2365–2367 (2008).
17. T. Wu, J. Liao, J. Yu, Y. Gao, H. Li, J. Wu, X. Xia, K. Shi, and W. Zheng, "In vivo label-free two-photon excitation autofluorescence microscopy of microvasculature using a 520 nm femtosecond fiber laser," *Opt. Lett.* **45**(10), 2704–2707 (2020).
18. C.-K. Tsai, Y.-S. Chen, P.-C. Wu, T.-Y. Hsieh, H.-W. Liu, C.-Y. Yeh, W.-L. Lin, J.-S. Chia, and T.-L. Liu, "Imaging granularity of leukocytes with third harmonic generation microscopy," *Biomed. Opt. Express* **3**(9), 2234–2243 (2012).
19. S. Maiti, J. B. Shear, R. Williams, W. Zipfel, and W. Webb, "Measuring serotonin distribution in live cells with three-photon excitation," *Science* **275**(5299), 530–532 (1997).
20. R. Chen, "Fluorescence quantum yields of tryptophan and tyrosine," *Anal. Lett.* **1**(1), 35–42 (1967).
21. B. Kierdaszuk, H. Malak, I. Gryczynski, P. Callis, and J. Lakowicz, "Fluorescence of reduced nicotinamides using one- and two-photon excitation," *Biophys. Chem.* **62**(1-3), 1–13 (1996).
22. J. R. Lakowicz, *Principles of Fluorescence Spectroscopy* (Springer, 2006).
23. O. Voloshina, E. Shirshin, J. Lademann, V. Fadeev, and M. Darvin, "Fluorescence detection of protein content in house dust: the possible role of keratin," *Indoor Air* **27**, 377–385 (2017).
24. D. Balasubramanian and R. Kanwar, "Molecular pathology of dityrosine cross-links in proteins: structural and functional analysis of four proteins," in *Oxygen/Nitrogen Radicals: Cell Injury and Disease* (Springer, 2002), pp. 27–38.
25. Z. Deyl, K. Macek, and M. J. Adam, "Studies on the chemical nature of elastin fluorescence," *Biochim. Biophys. Acta, Protein Struct.* **625**(2), 248–254 (1980).
26. J. Bridges, D. Davies, and R. Williams, "Fluorescence studies on some hydroxypyridines including compounds of the vitamin B6 group," *Biochem. J.* **98**(2), 451–468 (1966).
27. R. Richards-Kortum and E. Sevick-Muraca, "Quantitative optical spectroscopy for tissue diagnosis," *Annu. Rev. Phys. Chem.* **47**, 555–606 (1996).
28. R. E. Hirstch, "Hemoglobin fluorescence," in *Hemoglobin Disorders* (Springer, 2003), pp. 133–154.
29. A. B. Shrirao, R. S. Schloss, Z. Fritz, M. V. Shrirao, R. Rosen, M. L. J. B. Yarmush, and Bioengineering, "Autofluorescence of blood and its application in biomedical and clinical research," *Biotechnol. Bioeng.* **118**, 4550–4576 (2021).

30. I. Ashikawa, Y. Nishimura, M. Tsuboi, K. Watanabe, and K. Iso, "Lifetime of tyrosine fluorescence in nucleosome core particles," *J. Biochem.* **91**(6), 2047–2055 (1982).
31. J. Alcala, E. Gratton, and F. Prendergast, "Interpretation of fluorescence decays in proteins using continuous lifetime distributions," *Biophys. J.* **51**(6), 925–936 (1987).
32. J. R. Lakowicz, H. Szmajda, K. Nowaczyk, and M. L. Johnson, "Fluorescence lifetime imaging of free and protein-bound NADH," *Proc. Natl. Acad. Sci. U. S. A.* **89**(4), 1271–1275 (1992).
33. C. Bueno, P. Pavez, R. Salazar, M. Encinas, and photobiology, "Photophysics and photochemical studies of the vitamin B6 group and related derivatives," *Photochem. Photobiol.* **86**, 39–46 (2010).
34. M. Y. Berezin and S. Achilefu, "Fluorescence lifetime measurements and biological imaging," *Chem. Rev.* **110**(5), 2641–2684 (2010).
35. A. Ehlers, I. Riemann, M. Stark, and K. J. König, "Multiphoton fluorescence lifetime imaging of human hair," *Microsc. Res. Tech.* **70**, 154–161 (2007).
36. G. J. Smith, M. R. Thorpe, W. H. Melhuish, and G. Beddard, "Fluorescence of tryptophan in keratin," *Photochemistry and Photobiology* **32**, 715–718 (1980).
37. J. Albani, "Origin of tryptophan fluorescence lifetimes. Part 2: Fluorescence lifetimes origin of tryptophan in proteins," *J. Fluoresc.* **24**(1), 105–117 (2014).
38. C. Li, R. K. Pastila, C. Pitsillides, J. M. Runnels, M. Puoris'haag, D. Côté, and C. Lin, "Imaging leukocyte trafficking in vivo with two-photon-excited endogenous tryptophan fluorescence," *Opt. Express* **18**(2), 988–999 (2010).
39. C. Li, R. K. Pastila, and C. P. Lin, "Imaging immune response of skin mast cells in vivo with two-photon microscopy," in *Photonic Therapeutics and Diagnostics VIII*, (International Society for Optics and Photonics, 2012), 82070F.
40. C. Li, R. K. Pastila, and C. Lin, "Label-free imaging immune cells and collagen in atherosclerosis with two-photon and second harmonic generation microscopy," *J. Innov. Opt. Health Sci.* **09**(01), 1640003 (2016).